

Article

hERG Blockade Prediction by Combining Site Identification by Ligand Competitive Saturation and Physicochemical Properties

Himanshu Goel , Wenbo Yu and Alexander D. MacKerell, Jr. * 

Computer Aided Drug Design Center, Department of Pharmaceutical Sciences, University of Maryland School of Pharmacy, 20 Penn St., Baltimore, MD 21201, USA; hgoel@outerbanks.umaryland.edu (H.G.); wenbo@outerbanks.umaryland.edu (W.Y.)

* Correspondence: alex@outerbanks.umaryland.edu; Tel.: +1-410-706-7442

Abstract: The human ether-a-go-go-related gene (hERG) potassium channel is a well-known contributor to drug-induced cardiotoxicity and therefore is an extremely important target when performing safety assessments of drug candidates. Ligand-based approaches in connection with quantitative structure active relationships (QSAR) analyses have been developed to predict hERG toxicity. The availability of the recent published cryogenic electron microscopy (cryo-EM) structure for the hERG channel opened the prospect of using structure-based simulation and docking approaches for hERG drug liability predictions. In recent times, the idea of combining structure- and ligand-based approaches for modeling hERG drug liability has gained momentum offering improvements in predictability when compared to ligand-based QSAR practices alone. The present article demonstrates uniting the structure-based SILCS (site-identification by ligand competitive saturation) approach in conjunction with physicochemical properties to develop predictive models for hERG blockade. This combination leads to improved model predictability based on Pearson's R and percent correct (represents rank-ordering of ligands) metric for different validation sets of hERG blockers involving a diverse chemical scaffold and wide range of pIC₅₀ values. The inclusion of the SILCS structure-based approach allows determination of the hERG region to which compounds bind and the contribution of different chemical moieties in the compounds to the blockade, thereby facilitating the rational ligand design to minimize hERG liability.

Keywords: SILCS; hERG channel; physicochemical properties; multiple linear regression; FragMaps



Citation: Goel, H.; Yu, W.; MacKerell, A.D., Jr. hERG Blockade Prediction by Combining Site Identification by Ligand Competitive Saturation and Physicochemical Properties.

Chemistry **2022**, *4*, 630–646. <https://doi.org/10.3390/chemistry4030045>

Academic Editor: Edwin Charles Constable

Received: 17 May 2022

Accepted: 17 June 2022

Published: 21 June 2022

Publisher's Note: MDPI stays neutral with regard to jurisdictional claims in published maps and institutional affiliations.



Copyright: © 2022 by the authors. Licensee MDPI, Basel, Switzerland. This article is an open access article distributed under the terms and conditions of the Creative Commons Attribution (CC BY) license (<https://creativecommons.org/licenses/by/4.0/>).

1. Introduction

The hERG potassium channel plays an extremely important role in heart function by conducting the electrical activity of the heart. Blockade of the hERG channel can lead to QT interval (time measured in electrocardiogram from Q wave to end of T wave) prolongation (long QT syndrome), which can increase the risk of deadly cardiac arrhythmias or torsades de pointes (TdP) leading to sudden death [1–6]. Many drugs (e.g. astemizole, cisapride, sertindole, terfenadine, etc.) have been withdrawn from the market, or their usage restricted due to drug-induced arrhythmias and other side effects [7–9]. Therefore, hERG inhibition by drug candidates has become an important concern in pharmaceutical development [10,11]. Indeed, all potential drug candidates have to be scrutinized against the hERG channel to evaluate their consequences on heartbeat or other cardiovascular side effects as established by the Food and Drug Administration (FDA) and the European Medicine Agency (EMA) [11–15].

Given these complexities, *in silico* models offer the prospect of effectively eliminating potential drug candidates that could lead to hERG blockade, thereby saving the time and cost of drug development [16–20]. Moreover, a priori prediction of a compound's cardiotoxic potential would be of great utility during the early phase of the drug development process. In this context, a large number of ligand- or knowledge/machine learning

(ML)-based drug design models in the context of QSAR have been developed and successfully utilized to rapidly screen drug candidates for their ability to be a hERG binder or nonbinder [21–26]. Pharmacophore [27–30] and structure-based approaches employing homology models [31–34] are other avenues developed to filter drug candidates. A recent comprehensive review of hERG ligand structure activity relationships has been presented [35]. Moreover, the present-day ML-based models are getting better for classifying compounds, as indicated by improved correlation scores [36–44]. These models largely depend on the strong similarity of the candidate drugs to the chemical scaffold and/or different sets of properties used to train the models [45,46]. These methods would likely fail to recognize blockers from non-blockers when challenged by a novel compound whose structure or physicochemical properties are unrelated to the training set of ligands.

The availability of the cryo-EM structure of the hERG channel from Mackinnon and coworkers [47] unlocked the potential to use structure based drug design (SBDD) approaches for hERG screening of drug candidates. Beyond ligand-based methods, SBDD approaches may yield an understanding of the underlying atomistic interactions and binding orientations contributing to hERG binding and blockade. Accordingly, a number of research groups have applied structure-based simulation and docking approaches in modeling ligand interactions with hERG channels, revealing the benefits the SBDD approach can offer when compared to ligand-based techniques [48–57]. A contribution in this direction was recently reported by Mangiatordi and coworkers for a large number of compounds, where they showed the utility of docking scores and their integration with protein-ligand interaction fingerprints [58].

The Site Identification by Ligand Competitive Saturation (SILCS) technology is unique and innovative among SBDD approaches in that it applies a pre-computed ensemble strategy in a computer-aided drug design framework that produces accuracy similar to state of the art methods such as free energy perturbation while being hundreds of times more computationally efficient [59,60]. SILCS methodology involves running a combined oscillating chemical potential grand canonical Monte Carlo [61] and molecular dynamics simulation (GCMC/MD) of small solutes representing different chemical functionalities in the presence of the targeted protein in an explicit aqueous solution [61–63]. This results in generating functional group binding affinity patterns (FragMaps) based on the solute 3D probability distributions, which may then be used in the identification of druggable binding sites [64], for protein-ligand relative binding affinities [65–68], pharmacophore model development and database screening [69,70], to evaluate protein-protein interactions [71], facilitate the identification of excipients for biologics formulation [72,73], and identify the vital contribution of individual atoms and moieties contributing to ligand binding. A recent review article about different SILCS applications [74] can be referred to for additional details.

Taking advantage of the ability of SILCS to predict binding sites and relative affinities, in collaboration with the Noskov research group, the SILCS method was applied to the hERG structure 5VA1 and used to develop a SBDD predictive model of hERG blockade. In that study, which represents the methodological foundation for the present work, SILCS FragMaps were generated for hERG and used to identify binding sites on the channel into which 55 known blockers were docked and the relative affinities determined, allowing for correlation analysis with available experimental data. Results from the SILCS approach were compared to results from ligand binding using the GLIDE docking approach [75]. We move beyond that work in the present study by using the SILCS methodology singlehanded and in combination with ligand-based physicochemical properties for predicting the binding affinities and rank-ordering of the hERG blockers/non-blockers for a significantly wider variety of previously published hERG datasets than used in the original study.

As presented below, a major challenge to the development of successful hERG blockade models is a consistent database of hERG compounds with binding affinities measured using a uniform experimental protocol (experimental details, assay type, cell-lines, etc.) on a range of chemical scaffolds. To overcome this, we have accessed multiple previously

published compound sets curated with different emphases [24]. The training set includes a diverse collection of structural classes of compounds having a wide range in experimental pIC50 values from approximately two to eight. The accuracy of the SILCS-based models is then validated in modeling a wide range of hERG compounds coming from different sources [24,76,77]. In addition, we apply a Bayesian ML approach to improve the predictability of the SILCS model as well as combine the structure-based information with physicochemical properties. The resulting SBDD hERG blockade prediction models are equivalent to or slightly improved over LBDD ML models while having the benefit of the quantitative evaluation of the binding contributions of individual chemical moieties in the molecules, information available from the SILCS may be used to predict possible chemical modifications to limit hERG blockade.

2. Computational Details

The present study used the SILCS FragMaps calculated in our previous study of hERG blockade model development [75]. Briefly, the SILCS methodology involved running GCMC/MD simulations for the cryo-EM hERG structure (PDB 5VA1) [47] on which the regions not present in the structure had been modeled as previously described [78], in the presence of water and a set of solutes representing different chemical functionalities to generate the functional group affinity patterns (FragMaps) for all the solute molecules. The eight solutes were benzene, propane, methanol, formamide, acetaldehyde, imidazole, methylammonium, and acetate. The simulation system included the hERG channel surrounded in 2-oleoyl-1-palmitoyl-sn-glycero-3-phosphocholine (POPC) lipids along with cholesterol at a 9:1 ratio. From the SILCS simulations, normalized 3D probability distributions of the functional groups in the solutes encompassing the entire protein are obtained and converted into grid free energy (GFE) FragMaps based on Boltzmann transformation of the normalized probability distributions. The GFE FragMaps, listed in Table S1, Supporting Information, act as the basis for the SILCS-based SBDD. Details of the simulation setup, software, and FragMaps construction may be obtained from our previous hERG publication [75].

Ligand docking in the GFE FragMaps is performed using the SILCS-Monte Carlo (SILCS-MC) sampling method performed in the field of the GFE FragMaps. Docking was performed individually, targeting the previously identified S1 and S2 sites, both of which are located in the intracellular central cavity of hERG [79]. In a recent structure of hERG, the blocker astemizole was observed to bind in the vicinity of Y652, which is located in the S1 site. The SILCS-MC docking program involves running energy minimization, MC moves, and MC-simulated annealing steps on each ligand in the field of the FragMaps to obtain the lowest ligand grid free energy (LGFE) conformation and orientation of the ligand. LGFE values are the summation of the atomic GFE scores, where the GFE values are computed based on assigning a selected atom to a FragMap type and obtaining the atomic GFE scores based on the overlap of the ligand atoms and the corresponding FragMaps. The LGFE values are not formal absolute binding energies but are considered as an approximate representation of the experimental binding free energies. The predicted LGFE is converted to pIC50 values for comparison with the experimental values. The ligands were first energy minimized in the context of the CHARMM General Force Field energy function for 10,000 steps, followed by 10,000 MC steps at 300 K and 40,000 annealing steps from 300 to 0 K. The Monte Carlo moves include translations, rotations, and dihedral rotations of rotatable bonds that are accepted or rejected based on the Metropolis criteria. The Generic Apolar Scale Atomic Classification Scheme (GAS18 or 2018 Generic ACS) definitions are used for the FragMap classification of solute atoms (Table S1). The force field parameters for all the compounds were obtained from the CGenFF [80–82] program. Prior to SILCS-MC, the ligand is randomly placed in the radii of a user-specified radius (10 Å in either the S1 or S2 pocket). Five independent simulations of up to 50 MC runs for each ligand were carried out to improve sampling and obtain the minimum energy configuration based on convergence criteria of 0.5 kcal/mol or a maximum of 250 runs.

Improved predictability of the SILCS model was performed using the previously presented Bayesian machine learning (BML) optimization approach [67]. BML involves using Markov-chain Monte Carlo simulated annealing (MCSA) approach to optimize the weighting factors of the contributions of the FragMaps to the ligand LGFE scores used in the SILCS-MC docking platform. This method allows for the optimization of GFE contributions of the classified atom types from the different FragMap types, representing the features, resulting in maximizing either the Pearson's correlation (R) or percent correct (PC) metric targeting the experimental binding affinities of the ligands. The BML-optimized weights were then used to redock all the compounds in the training and validation sets from which the final R or PC metrics were obtained. In this study, the targeted error function is Pearson's R metric for determining new FragMap weights. The force constant for the flat bottom potential was set to 5000 kcal/mol with the lower (0.05) and upper (2.0) limits of FragMap weighting factors. Additional details on the SILCS-MC docking and BML optimization can be found in our earlier publications [65,67]. Furthermore, a simplified flow diagram has been shown in Figure S1 to depict the entire computational workflow.

The present study uses multiple sets of diverse ligands curated in previous studies as follows. Training was performed on a set of 163 compounds that includes diverse scaffolds and with standardized experimental pIC₅₀ values collected from different publications as described in our previous hERG publication [75]. The 163 blocker compounds were from the 700 compounds originally reported by Wacker et al. [24], selected based on chemical diversity [75]. For validation purposes, the initial test set of 55 compounds is taken from the work of Kramer et al. [76], where the IC₅₀ values were obtained from the same cell-line and similar experimental conditions. This blocker set contains well-known compounds varying from high to low binding affinities. Both the neutral and protonation states of all these compounds were considered, and corrections were made in the present study on the protonation states from those used in our previous work [75]. LGFE scores were obtained for both the neutral and charged states of the ionizable compounds. In addition to being used directly in model development, the LGFE scores from the two states were used to produce an ionization state weighted LGFE score by using the Henderson-Hasselbalch (HH) equation at pH = 7.4 as shown in our earlier publication [75]. Additional test sets of 77, 80, and 32 compounds were from Sinha et al. [77]. These data sets were carefully constructed to have compounds with wide ranges of pIC₅₀ values and a sufficient number of entries from each range of pIC₅₀ values to avoid biasing from over-representation. According to the authors, the patch clamp hERG current inhibition assay in the human embryonic kidney (HEK) or Chinese hamster ovary (CHO) cell lines was used to measure the experimental pIC₅₀ values for most of the compounds [77]. Finally, the different test sets compiled by Wacker et al. [24], comprised of a large number of compounds collected from the ChEMBL database, were used for additional model validation. The test sets 1, 3, and 4 contained 100, 155, and 73 compounds, respectively, collected from a large number of published articles. Overall, the collection of blockers in the training and validation sets, with the exception of the 55-blocker set, comes from different articles, thereby potentially leading to less consistency between the experimental binding data versus data coming from a single source obtained under similar biological conditions. The lack of consistency in these data sets impacts the ability of the developed models to predict their activity, as described below. The structures of all the blockers in the training and test sets, along with their binding affinities, are provided in the Supporting Information files.

A set of five physicochemical descriptors, namely partition coefficient (logP), solubility (logS), topological polar surface area (TPSA), molecular weight (MW), and van der Waals volume, were used to develop a multiple linear regression (MLR) model to predict activity both alone and in conjunction with the LGFE scores. The descriptor values were obtained from the Molecular Operating Environment (MOE) package (Chemical Computing Group) [83]. While additional descriptors can be included in an MLR-based or structure activity relationship model for further improvement of the correlation scores [84–86], this was

not undertaken as the goal of this study is to determine whether using common descriptors could benefit the predictability of the models.

Quantitative statistical evaluation of model predictability used multiple metrics. The metrics are mean unsigned error (MUE) between experimental and predicted pIC50 values, Pearson's R (R), predictive index (PI) [87], and percent correct (PC) metric. Pearson's R varies between -1 and 1 , denoting the quality of the fit and direction of the linear relationship between experimental and predicted values. The PI metric ranges between 1 and -1 , where 1 is for the 100% true relative predictions and -1 is for 100% false predictions, and 0 is for the random predictions, signifying the ability of the method to rank order the ligands based on their affinities. The sum of true positive and true negative comparisons for each series of ligands defines the PC metric. All the PC values are averaged values over individual PC values, with each compound in the series taken as the reference ligand. The PC metric is of utility in the context of lead optimization, where it can be used to select modifications with the potential to improve the desired target activity, in this case, decreased hERG binding.

3. Results and Discussion

Building on our previous study, the present work focused on systematically expanding the optimized model based on the 163-compound training set, including taking into account corrections to the ionization state of selected ligands (Supporting information). The developed models are then validated against a wider range of test data. These include more focused data sets with respect to compound types, experimental evaluation method, and publications from which they were obtained as well as test sets with more diverse compounds from a significantly larger number of publications. The final section presents the utility of the information content from the SILCS-based model that can be used in the rational design of compounds to minimize hERG liability.

3.1. SILCS-MC Docking for Training Set of 163 Compounds

Table 1 presents the statistical analysis based on the SILCS LGFE scores for the 163 blockers in S1 and S2 binding pockets with the standard FragMap weighting factors and the BML-optimized factors (Table S1, Supporting Information). The correlation scatters plot between the SILCS-predicted pIC50 scores versus the experimental pIC50 values with the BML-optimized weighting factors for both the binding pockets S1 and S2 is shown in Figure S2. Based on the LGFE scores alone, the predictive capabilities of the model are very low with the R and PI correlation terms approaching zero. However, the MUE values for both the S1 and S2 sites are approximately close to one, indicating that, while not yielding good correlations, the LGFE scores were giving a representative estimate of the overall binding affinities. Accordingly, the BML optimization operation was performed on the same set of 163 blockers in order to improve the predictability of the model. This approach acts to optimize the weighting of the different FragMap types (e.g., apolar, hydrogen bond donor, hydrogen bond acceptor, etc.) to improve the predictability of the model while maintaining the quality of the LGFE scores with respect to their ability to predict the magnitude of the pIC50 values. In this approach, the same FragMap weighting factors are applied to all the ligands, and importantly, the final results are based on redocking of the ligands into the reweighted SILCS FragMaps. This final step, along with the validation below, assures that the model is not being overfitted. When overfitting is performed, the new docked orientations deviate significantly from the original docked orientation, and the predictability of the model significantly diminishes. As may be seen in Table 1, BML optimization shows substantially improved performance of all the metrics, producing R values of 0.453/0.408 as compared to 0.108/0.044 for the S1 and S2 sites, respectively. Similarly, the average PC score of 0.643/0.605 is a substantial improvement over the initial values of 0.524/0.509. As mentioned in the above section, the 163 blockers include different scaffolds and a wide range of experimental pIC50 values taken from numerous publications having

different experimental conditions. Therefore, it represents a challenge for any docking or other ranking strategy to predict the ligand binding affinities.

Table 1. Statistical analysis for SILCS models developed based on the 163 hERG1 blockers in the S1 and S2 binding pockets with and without BML optimization.

Pocket	MUE	R	PI	PC
S1	0.836	0.108	0.097	0.524
S2	1.109	0.044	0.034	0.509
BML S1	0.903	0.453	0.456	0.643
BML S2	0.840	0.408	0.362	0.605

To select the final BML model for application to the remaining validation sets, the BML-weighted parameters were obtained by targeting 163 training ligands yielding individual S1 and S2 models and by taking minimum LGFE scores from both the pockets, yielding three sets of BML-optimized reweighted FragMaps. All three sets of reweighted FragMaps were tested against 55 neutral and 42 charged ligands. The best R/PC scores come from the S1 BML parameters when compared to others. Therefore, the BML-optimized parameters obtained from the training of 163 blockers in the S1 pocket were used for both the S1 and S2 binding sites in the analysis of the validation test sets presented below. The default and BML-optimized FragMap weighting factors are shown in Table S1 of the Supporting Information.

3.2. Application of SILCS-MC Predictive Models to Validation Sets

In this section, multiple ligand sets for validation purposes were used to test the SILCS-MC docking models with and without the BML-optimized parameters. The performance of average correlation scores for 55 hERG1 blockers in S1 and S2 binding pockets for neutral, charged, and HH-weighted scores are presented in Table 2 with and without BML optimization along with the physicochemical prediction model (PPM) and the combined consensus of PPM and SILCS LGFE scores. A multiple linear regression model was employed to consider the five parameters mentioned above. In addition, the three possibilities for treating the charge of the molecules are included in Table 2. The 55 blockers' pIC50 values were measured in the same cell-line and under similar experimental conditions and contained diverse scaffolds and a wide range of binding affinity values. As may be seen, the predictability of the SILCS models is improved over those optimized directly targeting the 163 compounds in the training set, though the two sets of compounds differ significantly (see Supporting Information Figures S3 and S4 and accompanying text). This emphasizes that using a single set of experimental data benefits to increase the consistency in the pIC50 values and supports the ability of the SILCS computational model to make consistent predictions. The outcomes from the BML-optimized model, in particular for Pearson's R, are substantially improved in all the states in the S1/S2 pockets when compared to our earlier publication for the same set of blockers after the protonation state corrections performed in this study (see Figure 6 of Mousaei et al. [75]). Furthermore, the performance of the models is sensitive to the ionization state of the compounds, with the neutral species yielding a more predictive model than the charged species and the HH-weighted model showing the best predictability. Thus, the SILCS BML model indicates the utility of the LGFE metric for predicting hERG blockade. Extending that model with physicochemical properties, yielding the consensus PPM + HH-weighted BML model, clearly shows large improvement as compared to the LGFE scores alone, signifying the contributions of the physicochemical properties. However, the PPM-only model produces a highly predictive model, approaching that of the consensus PPM-HH-weighted BML model, which is why LBDD hERG prediction approaches are so prevalent in the literature. Comparing the consensus and PPM-based model, the Pearson's score with BML S2 pocket for neutral, charged, and HH-weighted are 0.844, 0.815, and 0.834, whereas the PPM model produces 0.819, 0.784, and 0.809, respectively. Using the physicochemical properties in the consensus model

improves the performance of the MUE metric (approximately 0.7 log unit) for all the states in either the S1 or S2 pockets. The correlation scatter plot between the SILCS-predicted pIC50 scores versus the experimental pIC50 values with the BML consensus model is shown in Figure 1 for both the binding pockets S1 and S2. Overall, all the statistical analyses for the standard SILCS-MC and BML-optimized models show considerable improvement in the SILCS model with BML optimization, and using a few physicochemical descriptors further improves the predictability, showing the benefits from the combined structure- and ligand-based drug design approaches.

Table 2. Statistical analysis for 55 hERG1 blockers in S1 and S2 binding pockets for neutral, charged, and HH-weighted scores obtained using the models from the SILCS LGFE scores, PPM, and consensus SILCS-PPM ranking.

Docking Scores												
Pocket	Neutral State				Charged State				HH Weighted			
	MUE	R	PI	PC	MUE	R	PI	PC	MUE	R	PI	PC
S1	1.600	0.055	0.098	0.546	1.560	0.057	0.108	0.516	1.494	0.134	0.2	0.573
S2	1.745	0.099	0.114	0.546	1.759	0.092	0.179	0.542	1.682	0.15	0.187	0.573
BML S1	1.050	0.640	0.642	0.734	1.036	0.480	0.380	0.635	0.872	0.705	0.680	0.749
BML S2	1.349	0.611	0.579	0.708	1.329	0.476	0.443	0.653	1.179	0.632	0.619	0.722
PPM + Docking Scores												
S1	0.733	0.819	0.827	0.812	0.764	0.784	0.778	0.785	0.752	0.814	0.820	0.805
S2	0.709	0.825	0.825	0.815	0.743	0.792	0.787	0.794	0.721	0.824	0.828	0.816
BML S1	0.696	0.841	0.852	0.833	0.739	0.804	0.796	0.792	0.702	0.835	0.843	0.822
BML S2	0.669	0.844	0.847	0.826	0.704	0.815	0.763	0.780	0.693	0.834	0.818	0.811
PPM												
MLR	0.734	0.819	0.832	0.816	0.764	0.784	0.781	0.786	0.763	0.809	0.818	0.804

Additional validation sets containing 77, 80, and 32 compounds were obtained from the work of Sinha et al. These have a wide range of experimental pIC50 values from 2.46 to 8.21 and 2.36 to 8.66 and 1.59 to 8.17 for 77, 80, and 32 compounds, respectively. The average correlation scores for these datasets in S1 and S2 binding pockets are presented in Table 3 with standard and BML SILCS models along with the PPM only and consensus PPM/SILCS model. The BML model yields improved performance for the different metrics with all the datasets. The PPM-only model again produces quality predictions approaching but slightly worse than the BML/SILCS-based models. The Pearson's correlation with BML/S2 pocket for 77, 80, and 32 compounds are 0.722, 0.648, and 0.585, whereas the PPM model produces 0.691, 0.516, and 0.540, respectively. Figure 2 provides the scatter plots between the experimental and predicted pIC50 values for visual assessment of the BML consensus model based on the S1 and S2 pockets. The MUE accuracy of the BML consensus model for the 77 and 80 datasets varies between 0.71 and 0.78 log units, which is consistent with that of the 55 blockers. However, the 32 compound set yields a somewhat larger error, close to 1.3 log units, with lower performance of the other statistical metrics as compared to the outcomes from the 77 and 80 compound sets. The 32 compound set also showed a somewhat higher error (>1.6 log units) in the work of Sinha et al. [77] as well. The results from the SILCS and consensus model makes reasonable prediction for the 32 compounds, given their chemical diversity.

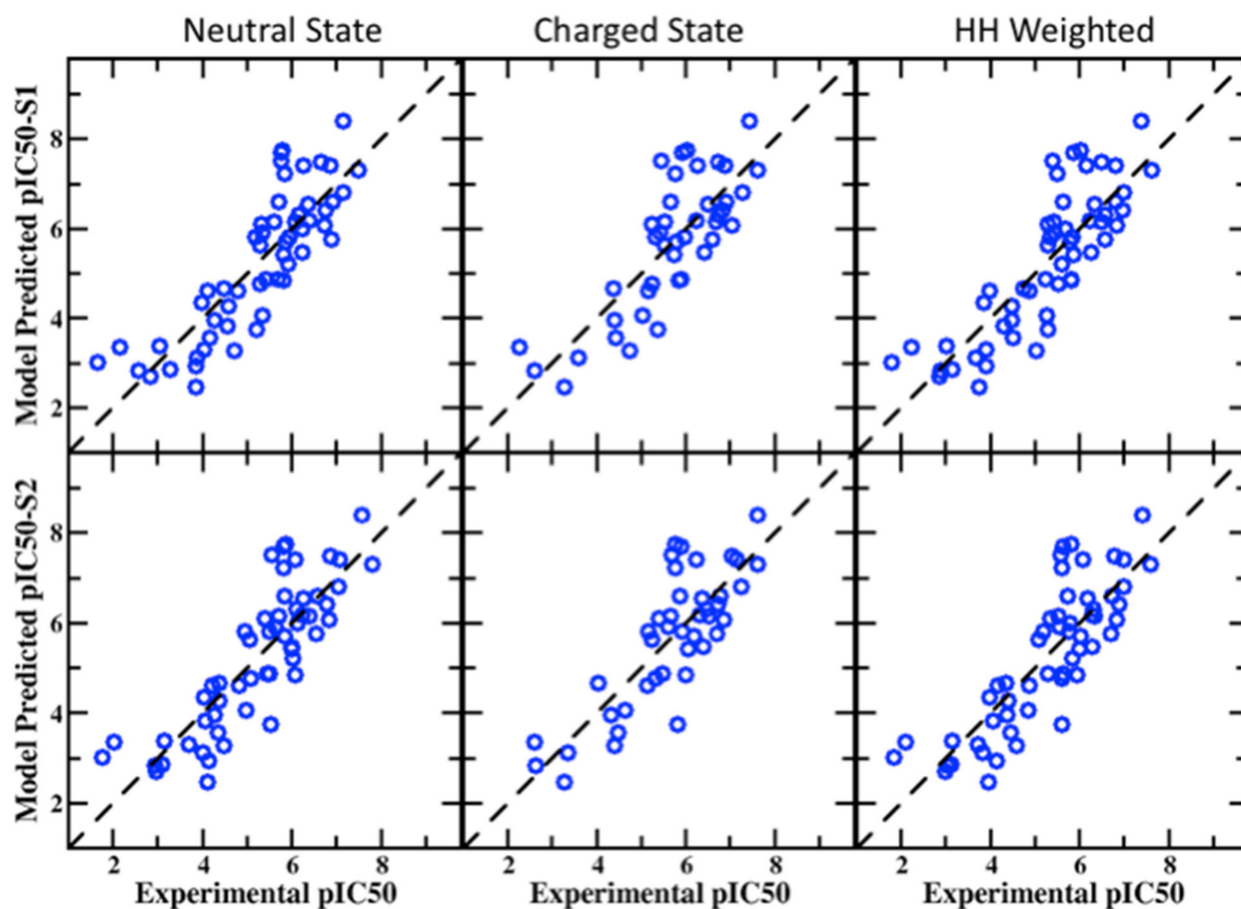


Figure 1. Correlation plots between experimental and predicted pIC50 values from the BML PPM + SILCS LGFE score consensus models for the neutral, charged, and HH-weighted in the S1 (top row) and S2 (bottom row) pockets in the hERG channel.

Table 3. Statistical analysis for 77, 80, and 32 blockers in S1 and S2 binding pockets using the models obtained from the SILCS LGFE scores, PPM, and consensus SILCS-PPM ranking.

Docking Scores												
Pocket	77 Compounds				80 Compounds				32 Compounds			
	MUE	R	PI	PC	MUE	R	PI	PC	MUE	R	PI	PC
S1	1.298	0.416	0.442	0.641	1.550	−0.078	0.066	0.511	1.888	0.235	0.267	0.589
S2	1.567	0.441	0.456	0.643	1.845	−0.014	0.143	0.549	2.055	0.227	0.297	0.607
BML S1	0.888	0.625	0.647	0.732	0.922	0.516	0.510	0.672	1.720	0.313	0.207	0.560
BML S2	1.185	0.646	0.659	0.738	1.345	0.532	0.541	0.686	1.904	0.363	0.392	0.613
Docking Scores + PPM												
S1	0.824	0.692	0.721	0.757	0.803	0.519	0.565	0.691	1.341	0.566	0.592	0.692
S2	0.822	0.691	0.707	0.749	0.796	0.529	0.575	0.699	1.315	0.562	0.549	0.679
BML S1	0.789	0.713	0.738	0.766	0.724	0.624	0.629	0.722	1.341	0.558	0.539	0.663
BML S2	0.775	0.722	0.745	0.771	0.711	0.648	0.642	0.725	1.320	0.585	0.560	0.681
PPM												
MLR	0.822	0.691	0.707	0.749	0.816	0.516	0.568	0.690	1.382	0.540	0.576	0.679

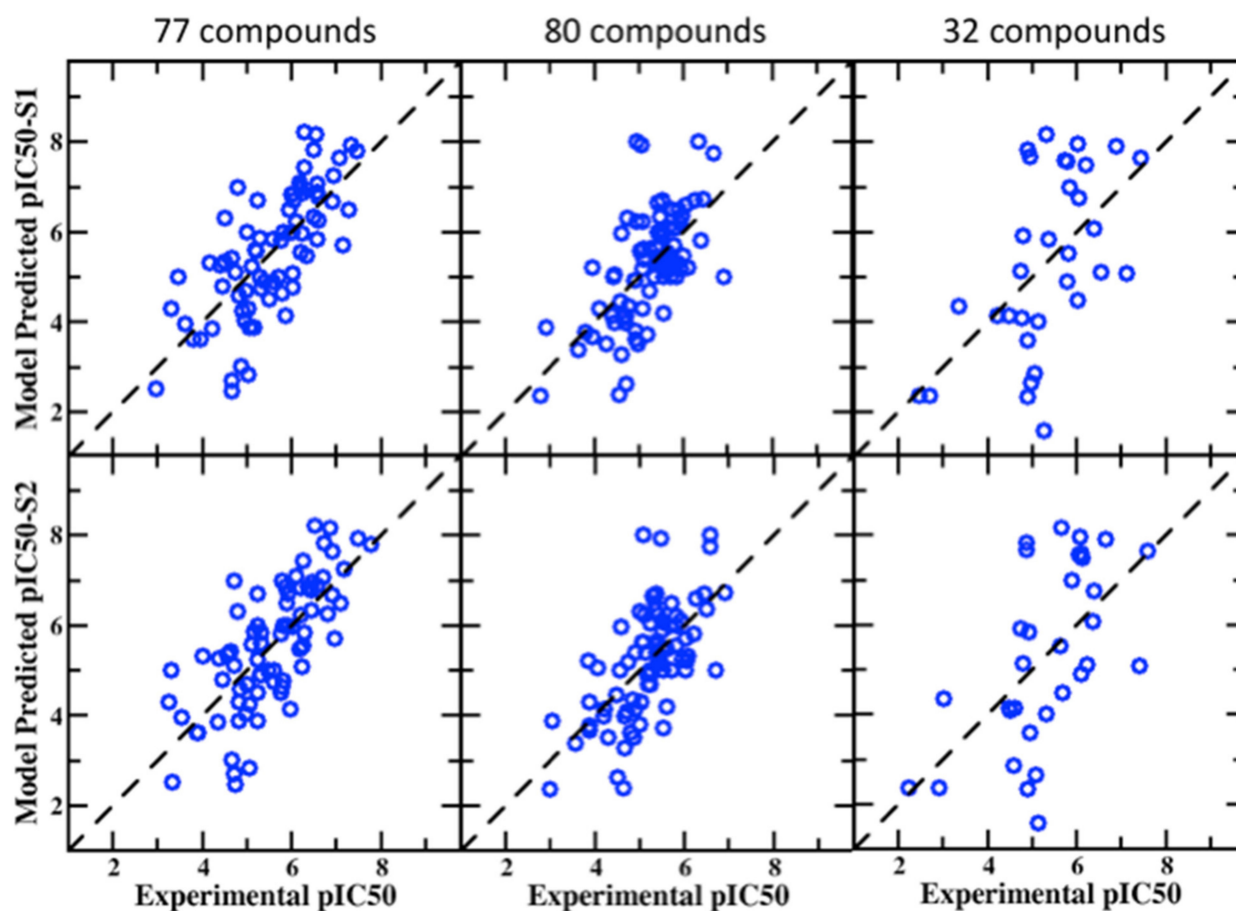


Figure 2. Correlation plots between experimental and predicted pIC50 values from the BML PPM + SILCS LGFE score consensus model for the 77, 80, and 32 compounds in the S1 (**top** row) and S2 (**bottom** row) pockets in the hERG channel.

The final three validation sets contain much more diverse ligands collected from various publications. The performance of different metrics for these validation sets is listed in Table 4, including standard and BML-optimized SILCS models along with the solely PPM and consensus PPM/SILCS model with the HH-weighted LGFE scores. The standard SILCS models provide negative or nil correlation for Pearson's R with all three datasets. The BML models make the predictions somewhat better and provide small positive correlations. Particularly, the prediction from the BML S1/S2 test one set is better than the other test sets. The consensus PPM/SILCS model further improves the correlation for all the datasets, with the standard and BML consensus models being similar. However, the correlation scores are highly similar to the PPM-only model. In other words, considering the binding affinity leads to no further improvement in the model predictability. This appears to be due to inconsistencies in the data as they were extracted from roughly 40, 60, and 80 publications for the 100, 155, and 73 compound sets, respectively [24]. In particular, every compound from test set four has a unique ChEMBL-assay ID after removal of the duplicates. This illustrates the extreme diversity of compounds in these datasets coming from different experimental procedures, making it difficult to deliver reliable predictions for any predictive model, as is seen by the improved prediction metrics in the test sets in Tables 2 and 3. Consistent with this, the Wacker et al. [24] article shows poor correlation performance for test sets three and four with their ML-based platform. The SILCS BML and SILCS/PPM consensus models make better predictions for both these test sets.

Table 4. Statistical analysis for Test sets 1, 3, and 4 in S1 and S2 binding pockets using the models obtained from the SILCS LGFE scores, PPM, and consensus SILCS-PPM ranking.

Docking Scores												
Pocket	Test 1 (100 Compounds)				Test 3 (155 Compounds)				Test 4 (73 Compounds)			
	MUE	R	PI	PC	MUE	R	PI	PC	MUE	R	PI	PC
S1	1.132	0.034	−0.001	0.503	1.021	−0.125	−0.161	0.464	0.888	−0.088	−0.073	0.476
S2	1.330	−0.019	−0.071	0.489	1.127	−0.156	−0.206	0.442	0.889	−0.159	−0.136	0.445
BML S1	1.008	0.242	0.247	0.608	0.868	0.092	0.105	0.555	1.084	0.061	0.094	0.534
BML S2	1.108	0.236	0.219	0.60	0.897	0.063	0.077	0.537	0.842	0.022	−0.002	0.500
Docking Scores + PPM												
S1	0.886	0.396	0.429	0.643	0.541	0.412	0.475	0.659	0.468	0.454	0.469	0.659
S2	0.937	0.325	0.329	0.595	0.541	0.413	0.474	0.658	0.470	0.444	0.463	0.658
BML S1	0.868	0.419	0.428	0.654	0.542	0.412	0.473	0.659	0.468	0.445	0.447	0.651
BML S2	0.866	0.416	0.43	0.656	0.543	0.412	0.481	0.660	0.468	0.445	0.449	0.651
PPM												
MLR	0.872	0.415	0.442	0.658	0.739	0.542	0.475	0.659	0.469	0.444	0.459	0.656

3.3. Molecular Conformation and Atomic GFE Contribution

The hERG channel can bind a wide range of molecules, making it difficult to understand the binding mode of the drug and the contribution of different moieties in the compounds to hERG binding. Earlier studies have shown that compounds can bind either parallel or perpendicular to the channel axis, and often, similar sets of residues play important roles in binding [88]. Mutation experiments confirm the crucial contributions of both polar (T623 and S624) and hydrophobic (Y652 and F656) residues to high affinity blockade [89–92]. However, ligand binding orientations may vary depending upon the functional state of the channel, mutated residues, and active/inactive channel conformations [88]. Therefore, understanding the role of different regions of ligands to hERG channel binding is quite challenging, making it difficult to rationally modify ligands in order to avoid the hERG liability.

The FragMaps obtained from the SILCS simulations, and the ligand conformations from the SILCS-MC docking can reveal the possible molecular interactions occurring between the ligand and protein residues that contribute to binding. This is revealed by the overlap of the SILCS FragMap types with different regions of the docked orientations of the ligands and a qualitative understanding of which protein residues contribute to those FragMaps. More quantitatively, the atomic GFE scores that are summed to yield the LGFE score allow for the free energy contributions of different regions of the ligands to the binding affinity to be determined. Thus, the SILCS docking approach allows for the identification of crucial atoms and functional group information that allows for the rational design of modifications to minimize binding to the hERG channel. This information can be of great use for lead optimization efforts and in understanding how different moieties of a compound contribute to the binding affinity. To exemplify this, the binding of two compounds from Gillman et al. [93] is shown in Figure 3. Figure 3A shows the minimum energy conformation of a compound in the region of hydrophobic residues Y652 and F656, indicating the importance of strong hydrophobic interactions. The FragMaps also identify the contribution of the protonated basic nitrogen through positive FragMaps, as shown in the center of Figure 3B,C which is consistent with the experimental predictions [94,95]. An example in this context is the cationic form of the antihistamine drug astemizole that overlapped with the positive FragMap, as shown in our previous work [75]. Moreover, Figure 3B,C presents a ΔpIC_{50} comparison between the minimum conformation of two congeneric ligands. The hydrophobic groups of the compounds occupy the SILCS apolar FragMaps on both sides, resulting in favorable GFE contributions from those groups.

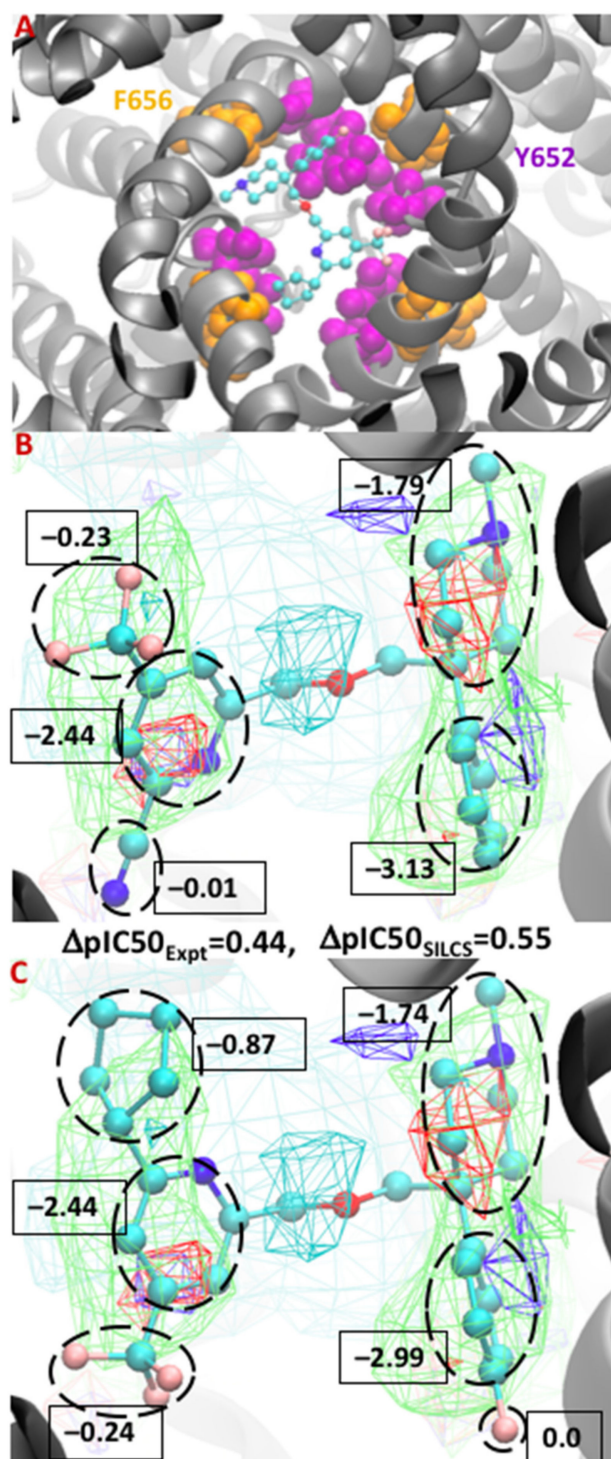


Figure 3. Binding orientation of a compound (from Gillman et al. [93]) in the S1 pocket in the vicinity of residues F656 and Y652 (A). Atomic GFE moiety contributions between the minimum conformation of the congeneric ligands 38 and 51 from test set 1 (B,C). The FragMaps colors are hydrophobic (GENN or APOLAR, green), hydrogen bond acceptor (GENA, red), hydrogen-bond donor (GEND, blue), and positive (MAMN, cyan). The FragMap isocontour surfaces are displayed at a cutoff of -0.8 kcal/mol for the apolar groups and rest of them at -1.0 kcal/mol. The atom cyan, blue, red, and pink colors represent carbon, nitrogen, oxygen, and fluorine atoms, respectively.

A comparison of the two ligands shows two modifications on each side of the congeneric molecules. On the right side of the molecule, the benzene ring of the ligand was

substituted with a fluorobenzene and on the left the cyano group is replaced with a cyclopentyl group. Upon going from the first to the second molecule, there is a $\sim 180^\circ$ rotation allowing the cyclopentyl group to make a favorable contribution due to overlapping with the apolar FragMaps (green) and occupying the hydrophobic pocket along with the connected pyridine ring. Overall, the modifications result in a computed $\Delta\text{pIC}_{50\text{SILCS}}$ score of 0.55 log units, matching well with the $\Delta\text{pIC}_{50\text{Expt}}$ value of 0.44 log units. The GFE contribution of the entire cyclopentyl group is -0.87 kcal/mol, making the dominant contribution to the change in affinity upon going from the compound in Figure 3B to the compound in Figure 3C. The GFE contribution of the pyridine ring remains identical in both the ligands, as does the trifluoromethyl group despite its change in position in the binding pocket. Interestingly, on the right side, the contribution of the fluorine atom is nil due to not having any acceptor FragMaps in that location, and there is no substantial difference in the summed GFE score of the fluorobenzene (-2.99 kcal/mol) versus the benzene ring (-3.13 kcal/mol). As is evident, the atomic GFE contributions can be of great use for efficiently designing the ligands with lowered hERG binding, information which is not accessible in other CADD binding affinity methods.

4. Conclusions

In the present article, an effective strategy of combining structure- and ligand-based drug design approaches is presented for modeling the relative binding of drug-like molecules to hERG. For this purpose, multiple validation sets were considered, and the ability of SILCS methodology was examined independently and in conjunction with simple physicochemical properties through MLR. The predictive model yields sensible performance for binding affinities, Pearson's correlation, and rank-ordering of the binding (percent correct) for different sets of hERG blockers, especially the ones which come from a single source or based on a consistent experimental setup. Therefore, consistency of the experimental data is very important for SBDD to satisfactorily predict relative affinities. The predictability of the BML-optimized SILCS model shows a large improvement in the performance when compared to the outcomes of standard SILCS-MC docking. It is important to emphasize that the reweighting of the FragMap contributions was performed only for the set of 163 blockers, with those weighting factors making satisfactory predictions for different validation datasets. Accordingly, the applicability domain of the developed model may be considered to encompass a wide range of structural classes given the overall predictability of the model for the different validation sets and given the diversity of the compounds in the 163 compound training set and the 55 compound validation set as determined from the Jaccard-Tanimoto similarity analysis (Supporting information Tables S3 and S4 and supporting text). Thus, the use of the presented model simply requires docking of novel ligands into the presented BML SILCS FragMaps, a process that requires only minutes, along with calculation of the required physicochemical properties. The SILCS software suite is available from SilcsBio LLC and is free of charge to academic users.

Similar to previous SILCS studies, the BML-optimization technique is an effective way to improve the predictability of the model, provided experimental information for the training set of ligands is available. Notably, this training set can be small, approaching ten molecules, as shown in our previous studies [65,67]. In addition, the predictability is enhanced with the addition of physicochemical molecular descriptors. Thus, the SILCS SBDD predictive model alone cannot handle hERG compounds obtained from diverse studies. This is consistent with studies showing the need to use specific ML classifier algorithms for handling miscellaneous sets of compounds based on the varied binding mode (e.g., parallel, perpendicular or alternate orientation), diverse experimental range of pIC_{50} values, and diverse chemical scaffold as shown in the literature [19,88]. Altogether, the SILCS methodology integrated with few physicochemical properties offers the benefit of predicting relative hERG blockade while providing the advantage of quantitatively understanding how individual moieties in a compound contribute to the change in binding affinity, information that may be used to rationally limit hERG binding.

Supplementary Materials: The following supporting information can be downloaded at: <https://www.mdpi.com/article/10.3390/chemistry4030045/s1>, Figure S1: Flow diagram for the entire SILCS workflow; Figure S2: Correlation plots for the BML SILCS predicted vs experimental pIC50 values for the 163 training ligands; Figure S3: Extended Jaccard-Tanimoto (JT) similarity index versus coincidence threshold for the 163 molecules set; Figure S4: Diversity versus coincidence threshold for the 163 molecules set; Table S1: The atom type classification weighting factors of the SILCS FragMaps for the default 2018 ACS and BML-Optimized [96–98].

Author Contributions: Data curation, H.G.; Formal analysis, H.G. and W.Y.; Funding acquisition, A.D.M.J.; Investigation, H.G.; Methodology, H.G., W.Y. and A.D.M.J.; Project administration, A.D.M.J.; Resources, A.D.M.J.; Software, W.Y.; Supervision, A.D.M.J.; Validation, H.G. and A.D.M.J.; Visualization, H.G.; Writing—original draft, H.G.; Writing—review and editing, H.G., W.Y. and A.D.M.J. All authors have read and agreed to the published version of the manuscript.

Funding: This research work was supported by NIH grant R35GM131710 and the Samuel Waxman Cancer Research Foundation.

Data Availability Statement: Information GitHub access of the SDF files and experimental data, etc. <https://github.com/mackerell-lab/Herg-Ligands> (accessed on 16 May 2022).

Acknowledgments: The authors acknowledge computer time and resources from the Computer-Aided Drug Design (CADD) Center at the University of Maryland, Baltimore. We also would like to pay tribute to a great academician and scientist, Sergei Noskov. He will be remembered always for his outstanding contributions.

Conflicts of Interest: A.D.M.J. is co-founder and Chief Scientific Officer of SilcsBio LLC.

References

1. Redfern, W.; Carlsson, L.; Davis, A.; Lynch, W.; MacKenzie, I.; Palethorpe, S.; Siegl, P.; Strang, I.; Sullivan, A.; Wallis, R. Relationships between preclinical cardiac electrophysiology, clinical QT interval prolongation and torsade de pointes for a broad range of drugs: Evidence for a provisional safety margin in drug development. *Cardiovasc. Res.* **2003**, *58*, 32–45. [[CrossRef](#)]
2. Priest, B.; Bell, I.M.; Garcia, M. Role of hERG potassium channel assays in drug development. *Channels* **2008**, *2*, 87–93. [[CrossRef](#)] [[PubMed](#)]
3. De Bruin, M.L.; Pettersson, M.; Meyboom, R.H.; Hoes, A.W.; Leufkens, H.G. Anti-HERG activity and the risk of drug-induced arrhythmias and sudden death. *Eur. Heart J.* **2005**, *26*, 590–597. [[CrossRef](#)] [[PubMed](#)]
4. Ray, W.A.; Murray, K.T.; Meredith, S.; Narasimhulu, S.S.; Hall, K.; Stein, C.M. Oral erythromycin and the risk of sudden death from cardiac causes. *N. Engl. J. Med.* **2004**, *351*, 1089–1096. [[CrossRef](#)] [[PubMed](#)]
5. Killeen, M.J. Drug-induced arrhythmias and sudden cardiac death: Implications for the pharmaceutical industry. *Drug Discov. Today* **2009**, *14*, 589–597. [[CrossRef](#)]
6. Nachimuthu, S.; Assar, M.D.; Schussler, J.M. Drug-induced QT interval prolongation: Mechanisms and clinical management. *Ther. Adv. Drug Saf.* **2012**, *3*, 241–253. [[CrossRef](#)]
7. Onakpoya, I.J.; Heneghan, C.J.; Aronson, J.K. Post-marketing withdrawal of 462 medicinal products because of adverse drug reactions: A systematic review of the world literature. *BMC Med.* **2016**, *14*, 1–11. [[CrossRef](#)]
8. Jamieson, C.; Moir, E.M.; Rankovic, Z.; Wishart, G. Medicinal chemistry of hERG optimizations: Highlights and hang-ups. *J. Med. Chem.* **2006**, *49*, 5029–5046. [[CrossRef](#)]
9. Roden, D.M. Drug-induced prolongation of the QT interval. *N. Engl. J. Med.* **2004**, *350*, 1013–1022. [[CrossRef](#)]
10. Fermini, B.; Fossa, A.A. The impact of drug-induced QT interval prolongation on drug discovery and development. *Nat. Rev. Drug Discov.* **2003**, *2*, 439–447. [[CrossRef](#)]
11. Garrido, A.; Lepailleur, A.; Mignani, S.M.; Dallemagne, P.; Rochais, C. hERG toxicity assessment: Useful guidelines for drug design. *Eur. J. Med. Chem.* **2020**, *195*, 112290. [[CrossRef](#)] [[PubMed](#)]
12. Strauss, D.G.; Gintant, G.; Li, Z.; Wu, W.; Blinova, K.; Vicente, J.; Turner, J.R.; Sager, P.T. Comprehensive in vitro proarrhythmia assay (CiPA) update on a cardiac safety research consortium/health and environmental sciences institute/FDA meeting. *Ther. Innov. Regul. Sci.* **2019**, *53*, 519–525. [[CrossRef](#)] [[PubMed](#)]
13. Vicente, J.; Zusterzeel, R.; Johannesen, L.; Mason, J.; Sager, P.; Patel, V.; Matta, M.K.; Li, Z.; Liu, J.; Garnett, C. Mechanistic model-informed proarrhythmic risk assessment of drugs: Review of the “CiPA” initiative and design of a prospective clinical validation study. *Clin. Pharmacol. Ther.* **2018**, *103*, 54–66. [[CrossRef](#)]
14. Chi, K.R. Revolution dawning in cardiotoxicity testing. *Nat. Rev. Drug Discov.* **2013**, *12*, 565. [[CrossRef](#)] [[PubMed](#)]
15. Colatsky, T.; Fermini, B.; Gintant, G.; Pierson, J.B.; Sager, P.; Sekino, Y.; Strauss, D.G.; Stockbridge, N. The comprehensive in vitro proarrhythmia assay (CiPA) initiative—Update on progress. *J. Pharmacol. Toxicol. Methods* **2016**, *81*, 15–20. [[CrossRef](#)] [[PubMed](#)]
16. Aronov, A.M. Predictive in silico modeling for hERG channel blockers. *Drug Discov. Today* **2005**, *10*, 149–155. [[CrossRef](#)]

17. Villoutreix, B.O.; Taboureau, O. Computational investigations of hERG channel blockers: New insights and current predictive models. *Adv. Drug Deliv. Rev.* **2015**, *86*, 72–82. [[CrossRef](#)]
18. Jing, Y.; Easter, A.; Peters, D.; Kim, N.; Enyedy, I.J. In silico prediction of hERG inhibition. *Future Med. Chem.* **2015**, *7*, 571–586. [[CrossRef](#)]
19. Kalyaanamoorthy, S.; Barakat, K.H. Development of safe drugs: The hERG challenge. *Med. Res. Rev.* **2018**, *38*, 525–555. [[CrossRef](#)]
20. Song, M.; Clark, M. Development and evaluation of an in silico model for hERG binding. *J. Chem. Inf. Model.* **2006**, *46*, 392–400. [[CrossRef](#)]
21. Thai, K.-M.; Ecker, G.F. A binary QSAR model for classification of hERG potassium channel blockers. *Bioorg. Med. Chem.* **2008**, *16*, 4107–4119. [[CrossRef](#)]
22. Hemmerich, J.; Ecker, G.F. In silico toxicology: From structure–activity relationships towards deep learning and adverse outcome pathways. *WIREs Comput. Mol. Sci.* **2020**, *10*, e1475. [[CrossRef](#)]
23. Wang, S.; Sun, H.; Liu, H.; Li, D.; Li, Y.; Hou, T. ADMET evaluation in drug discovery. 16. Predicting hERG blockers by combining multiple pharmacophores and machine learning approaches. *Mol. Pharm.* **2016**, *13*, 2855–2866. [[CrossRef](#)] [[PubMed](#)]
24. Wacker, S.; Noskov, S.Y. Performance of machine learning algorithms for qualitative and quantitative prediction drug blockade of hERG1 channel. *Comput. Toxicol.* **2018**, *6*, 55–63. [[CrossRef](#)] [[PubMed](#)]
25. Braga, R.C.; Alves, V.M.; Silva, M.F.B.; Muratov, E.; Fourches, D.; Tropsha, A.; Andrade, C.H. Tuning HERG out: Antitarget QSAR models for drug development. *Curr. Top. Med. Chem.* **2014**, *14*, 1399–1415. [[CrossRef](#)] [[PubMed](#)]
26. Seierstad, M.; Agrafiotis, D.K. A QSAR model of hERG binding using a large, diverse, and internally consistent training set. *Chem. Biol. Drug Des.* **2006**, *67*, 284–296. [[CrossRef](#)] [[PubMed](#)]
27. Kratz, J.M.; Schuster, D.; Edtbauer, M.; Saxena, P.; Mair, C.E.; Kirchebner, J.; Matuszczak, B.; Baburin, I.; Hering, S.; Rollinger, J.M. Experimentally validated hERG pharmacophore models as cardiotoxicity prediction tools. *J. Chem. Inf. Model.* **2014**, *54*, 2887–2901. [[CrossRef](#)] [[PubMed](#)]
28. Yamakawa, Y.; Furutani, K.; Inanobe, A.; Ohno, Y.; Kurachi, Y. Pharmacophore modeling for hERG channel facilitation. *Biochem. Biophys. Res. Commun.* **2012**, *418*, 161–166. [[CrossRef](#)]
29. Cavalli, A.; Poluzzi, E.; De Ponti, F.; Recanatini, M. Toward a pharmacophore for drugs inducing the long QT syndrome: Insights from a CoMFA study of HERG K⁺ channel blockers. *J. Med. Chem.* **2002**, *45*, 3844–3853. [[CrossRef](#)]
30. Munawar, S.; Windley, M.J.; Tse, E.G.; Todd, M.H.; Hill, A.P.; Vandenberg, J.I.; Jabeen, I. Experimentally validated pharmacoinformatics approach to predict hERG inhibition potential of new chemical entities. *Front. Pharmacol.* **2018**, *9*, 1035. [[CrossRef](#)]
31. Pagadala, N.S. Computational prediction of hERG blockers using homology modelling, molecular docking and QuaSAR studies. *Results Chem.* **2021**, *3*, 100101. [[CrossRef](#)]
32. Rajamani, R.; Tounge, B.A.; Li, J.; Reynolds, C.H. A two-state homology model of the hERG K⁺ channel: Application to ligand binding. *Bioorg. Med. Chem. Lett.* **2005**, *15*, 1737–1741. [[CrossRef](#)]
33. Farid, R.; Day, T.; Friesner, R.A.; Pearlstein, R.A. New insights about HERG blockade obtained from protein modeling, potential energy mapping, and docking studies. *Bioorg. Med. Chem.* **2006**, *14*, 3160–3173. [[CrossRef](#)]
34. Durdagi, S.; Deshpande, S.; Duff, H.J.; Noskov, S.Y. Modeling of open, closed, and open-inactivated states of the hERG1 channel: Structural mechanisms of the state-dependent drug binding. *J. Chem. Inf. Model.* **2012**, *52*, 2760–2774. [[CrossRef](#)] [[PubMed](#)]
35. Cavalluzzi, M.M.; Imbrici, P.; Gualdani, R.; Stefanachi, A.; Mangiatordi, G.F.; Lentini, G.; Nicolotti, O. Human ether-à-go-go-related potassium channel: Exploring SAR to improve drug design. *Drug Discov. Today* **2020**, *25*, 344–366. [[CrossRef](#)] [[PubMed](#)]
36. Lee, H.-M.; Yu, M.-S.; Kazmi, S.R.; Oh, S.Y.; Rhee, K.-H.; Bae, M.-A.; Lee, B.H.; Shin, D.-S.; Oh, K.-S.; Ceong, H. Computational determination of hERG-related cardiotoxicity of drug candidates. *BMC Bioinf.* **2019**, *20*, 67–73. [[CrossRef](#)]
37. Zhang, Y.; Zhao, J.; Wang, Y.; Fan, Y.; Zhu, L.; Yang, Y.; Chen, X.; Lu, T.; Chen, Y.; Liu, H. Prediction of hERG K⁺ channel blockage using deep neural networks. *Chem. Biol. Drug Des.* **2019**, *94*, 1973–1985. [[CrossRef](#)]
38. Czodrowski, P. hERG me out. *J. Chem. Inf. Model.* **2013**, *53*, 2240–2251. [[CrossRef](#)]
39. Konda, L.S.K.; Praba, S.K.; Kristam, R. hERG liability classification models using machine learning techniques. *Comput. Toxicol.* **2019**, *12*, 100089. [[CrossRef](#)]
40. Ryu, J.Y.; Lee, M.Y.; Lee, J.H.; Lee, B.H.; Oh, K.-S. DeepHIT: A deep learning framework for prediction of hERG-induced cardiotoxicity. *Bioinformatics* **2020**, *36*, 3049–3055. [[CrossRef](#)]
41. Wang, Y.; Huang, L.; Jiang, S.; Wang, Y.; Zou, J.; Fu, H.; Yang, S. Capsule networks showed excellent performance in the classification of hERG blockers/nonblockers. *Front. Pharmacol.* **2020**, *10*, 1631. [[CrossRef](#)] [[PubMed](#)]
42. Yang, Y.; Zhang, Y.; Chen, X.; Hua, Y.; Xing, G.; Deng, C.; Liang, L.; Lu, T.; Chen, Y.; Liu, H. Reducing hERG Toxicity Using hERG Classification Model and Fragment-growing Network. *ChemRxiv* **2021**. [[CrossRef](#)]
43. Chavan, S.; Abdelaziz, A.; Wiklander, J.G.; Nicholls, I.A. A k-nearest neighbor classification of hERG K⁺ channel blockers. *J. Comput. Aided Mol. Des.* **2016**, *30*, 229–236. [[CrossRef](#)] [[PubMed](#)]
44. Siramshetty, V.B.; Chen, Q.; Devarakonda, P.; Preissner, R. The Catch-22 of predicting hERG blockade using publicly accessible bioactivity data. *J. Chem. Inf. Model.* **2018**, *58*, 1224–1233. [[CrossRef](#)]
45. Gadaleta, D.; Mangiatordi, G.F.; Catto, M.; Carotti, A.; Nicolotti, O. Applicability domain for QSAR models: Where theory meets reality. *Int. J. Quant. Struct.-Prop. Relat.* **2016**, *1*, 45–63. [[CrossRef](#)]

46. Schyman, P.; Liu, R.; Wallqvist, A. General purpose 2D and 3D similarity approach to identify hERG blockers. *J. Chem. Inf. Model.* **2016**, *56*, 213–222. [[CrossRef](#)]
47. Wang, W.; MacKinnon, R. Cryo-EM structure of the open human ether-à-go-go-related K⁺ channel hERG. *Cell* **2017**, *169*, 422–430.e410. [[CrossRef](#)]
48. Dickson, C.J.; Velez-Vega, C.; Duca, J.S. Revealing molecular determinants of hERG blocker and activator binding. *J. Chem. Inf. Model.* **2019**, *60*, 192–203. [[CrossRef](#)]
49. Helliwell, M.V.; Zhang, Y.; El Harchi, A.; Du, C.; Hancox, J.C.; Dempsey, C.E. Structural implications of hERG K⁺ channel block by a high-affinity minimally structured blocker. *J. Biol. Chem.* **2018**, *293*, 7040–7057. [[CrossRef](#)]
50. Negami, T.; Araki, M.; Okuno, Y.; Terada, T. Calculation of absolute binding free energies between the hERG channel and structurally diverse drugs. *Sci. Rep.* **2019**, *9*, 1–12. [[CrossRef](#)]
51. Munawar, S.; Vandenberg, J.I.; Jabeen, I. Molecular Docking Guided Grid-Independent Descriptor Analysis to Probe the Impact of Water Molecules on Conformational Changes of hERG Inhibitors in Drug Trapping Phenomenon. *Int. J. Mol. Sci.* **2019**, *20*, 3385. [[CrossRef](#)]
52. Perissinotti, L.; Guo, J.; Kudaibergenova, M.; Lees-Miller, J.; Ol'khovich, M.; Sharapova, A.; Perlovich, G.L.; Muruve, D.A.; Gerull, B.; Noskov, S.Y. The pore-lipid interface: Role of amino-Acid determinants of lipophilic access by ivabradine to the hERG1 pore domain. *Mol. Pharmacol.* **2019**, *96*, 259–271. [[CrossRef](#)] [[PubMed](#)]
53. Zangerl-Plessl, E.-M.; Berger, M.; Drescher, M.; Chen, Y.; Wu, W.; Maulide, N.; Sanguinetti, M.; Stary-Weinzinger, A. Toward a Structural View of hERG Activation by the Small-Molecule Activator ICA-105574. *J. Chem. Inf. Model.* **2019**, *60*, 360–371. [[CrossRef](#)] [[PubMed](#)]
54. Kudaibergenova, M.; Guo, J.; Khan, H.M.; Zahid, F.; Lees-Miller, J.; Noskov, S.Y.; Duff, H.J. Allosteric Coupling Between Drug Binding and the Aromatic Cassette in the Pore Domain of the hERG1 Channel: Implications for a State-Dependent Blockade. *Front. Pharmacol.* **2020**, *11*, 914. [[CrossRef](#)] [[PubMed](#)]
55. Kalyaanamoorthy, S.; Lamothe, S.M.; Hou, X.; Moon, T.C.; Kurata, H.T.; Houghton, M.; Barakat, K.H. A structure-based computational workflow to predict liability and binding modes of small molecules to hERG. *Sci. Rep.* **2020**, *10*, 1–18. [[CrossRef](#)]
56. Wan, H.; Selvaggio, G.; Pearlstein, R.A. Toward in vivo-relevant hERG safety assessment and mitigation strategies based on relationships between non-equilibrium blocker binding, three-dimensional channel-blocker interactions, dynamic occupancy, dynamic exposure, and cellular arrhythmia. *PLoS ONE* **2020**, *15*, e0234946. [[CrossRef](#)]
57. Schewe, M.; Sun, H.; Mert, Ü.; Mackenzie, A.; Pike, A.C.; Schulz, F.; Constantin, C.; Vowinkel, K.S.; Conrad, L.J.; Kiper, A.K. A pharmacological master key mechanism that unlocks the selectivity filter gate in K⁺ channels. *Science* **2019**, *363*, 875–880. [[CrossRef](#)]
58. Creanza, T.M.; Delre, P.; Ancona, N.; Lentini, G.; Saviano, M.; Mangiatordi, G.F. Structure-Based Prediction of hERG-Related Cardiotoxicity: A Benchmark Study. *J. Chem. Inf. Model.* **2021**, *61*, 4758–4770. [[CrossRef](#)]
59. Guvench, O.; MacKerell, A.D., Jr. Computational fragment-based binding site identification by ligand competitive saturation. *PLoS Comput. Biol.* **2009**, *5*, e1000435. [[CrossRef](#)]
60. Faller, C.E.; Raman, E.P.; MacKerell, A.D.; Guvench, O. Site Identification by Ligand Competitive Saturation (SILCS) simulations for fragment-based drug design. In *Fragment-Based Methods in Drug Discovery*; Springer: New York, NY, USA, 2015; pp. 75–87.
61. Lakkaraju, S.K.; Raman, E.P.; Yu, W.; MacKerell, A.D., Jr. Sampling of Organic Solutes in Aqueous and Heterogeneous Environments using Oscillating μ ex Grand Canonical-like Monte Carlo-Molecular Dynamics Simulations. *J. Chem. Theory Comput.* **2014**, *10*, 2281–2290. [[CrossRef](#)]
62. Raman, E.P.; Yu, W.; Guvench, O.; MacKerell, A.D. Reproducing crystal binding modes of ligand functional groups using Site-Identification by Ligand Competitive Saturation (SILCS) simulations. *J. Chem. Inf. Model.* **2011**, *51*, 877–896. [[CrossRef](#)] [[PubMed](#)]
63. Raman, E.P.; Yu, W.; Lakkaraju, S.K.; MacKerell, A.D., Jr. Inclusion of Multiple Fragment Types in the Site Identification by Ligand Competitive Saturation (SILCS) Approach. *J. Chem. Inf. Model.* **2013**, *53*, 3384–3398. [[CrossRef](#)] [[PubMed](#)]
64. MacKerell, A.D., Jr.; Jo, S.; Lakkaraju, S.K.; Lind, C.; Yu, W. Identification and characterization of fragment binding sites for allosteric ligand design using the site identification by ligand competitive saturation hotspots approach (SILCS-Hotspots). *Biochim. Biophys. Acta Gen. Subj.* **2020**, *1864*, 129519. [[CrossRef](#)] [[PubMed](#)]
65. Goel, H.; Hazel, A.; Ustach, V.D.; Jo, S.; Yu, W.; Mackerell, A. Rapid and Accurate Estimation of Protein-Ligand Relative Binding Affinities using Site-Identification by Ligand Competitive Saturation. *Chem. Sci.* **2021**, *12*, 8844–8858. [[CrossRef](#)] [[PubMed](#)]
66. Goel, H.; Yu, W.; Ustach, V.D.; Aytenfisu, A.H.; Sun, D.; MacKerell, A.D. Impact of electronic polarizability on protein-functional group interactions. *Phys. Chem. Chem. Phys.* **2020**, *22*, 6848–6860. [[CrossRef](#)]
67. Ustach, V.D.; Lakkaraju, S.K.; Jo, S.; Yu, W.; Jiang, W.; MacKerell, A.D., Jr. Optimization and Evaluation of Site-Identification by Ligand Competitive Saturation (SILCS) as a Tool for Target-Based Ligand Optimization. *J. Chem. Inf. Model.* **2019**, *59*, 3018–3035. [[CrossRef](#)]
68. Raman, E.P.; Lakkaraju, S.K.; Denny, R.A.; MacKerell, A.D., Jr. Estimation of relative free energies of binding using pre-computed ensembles based on the single-step free energy perturbation and the site-identification by Ligand competitive saturation approaches. *J. Comput. Chem.* **2017**, *38*, 1238–1251. [[CrossRef](#)]
69. Yu, W.; Lakkaraju, S.K.; Raman, E.P.; Fang, L.; MacKerell, A.D., Jr. Pharmacophore Modeling Using Site-Identification by Ligand Competitive Saturation (SILCS) with Multiple Probe Molecules. *J. Chem. Inf. Model.* **2015**, *55*, 407–420. [[CrossRef](#)]

70. Yu, W.; Lakkaraju, S.K.; Raman, E.P.; MacKerell, A.D., Jr. Site-Identification by Ligand Competitive Saturation (SILCS) assisted pharmacophore modeling. *J. Comput. Aided Mol. Des.* **2014**, *28*, 491–507. [[CrossRef](#)]
71. Yu, W.; Jo, S.; Lakkaraju, S.K.; Weber, D.J.; MacKerell, A.D., Jr. Exploring protein-protein interactions using the Site-Identification by Ligand Competitive Saturation (SILCS) methodology. *Proteins Struct. Funct. Bioinf.* **2019**, *87*, 289–301. [[CrossRef](#)]
72. Jo, S.; Xu, A.; Curtis, J.E.; Somani, S.; MacKerell, A.D. Computational Characterization of Antibody-Excipient Interactions for Rational Excipient Selection using the Site Identification by Ligand Competitive Saturation (SILCS)-Biologics Approach. *Mol. Pharm.* **2020**, *17*, 4323–4333. [[CrossRef](#)] [[PubMed](#)]
73. Somani, S.; Jo, S.; Thirumangalathu, R.; Rodrigues, D.; Tanenbaum, L.M.; Amin, K.; MacKerell, A.D., Jr.; Thakkar, S.V. Toward biotherapeutics formulation composition Engineering using site-identification by ligand competitive saturation (SILCS). *J. Pharm. Sci.* **2021**, *110*, 1103–1110. [[CrossRef](#)] [[PubMed](#)]
74. Goel, H.; Hazel, A.; Yu, W.; Jo, S.; MacKerell, A.D. Application of site-identification by ligand competitive saturation in computer-aided drug design. *New J. Chem.* **2022**, *46*, 919–932. [[CrossRef](#)]
75. Mousaei, M.; Kudaibergenova, M.; MacKerell, A.D., Jr.; Noskov, S. Assessing hERG1 blockade from Bayesian machine-learning-optimized site identification by ligand competitive saturation simulations. *J. Chem. Inf. Model.* **2020**, *60*, 6489–6501. [[CrossRef](#)] [[PubMed](#)]
76. Kramer, J.; Obejero-Paz, C.A.; Myatt, G.; Kuryshv, Y.A.; Bruening-Wright, A.; Verducci, J.S.; Brown, A.M. MICE models: Superior to the HERG model in predicting Torsade de Pointes. *Sci. Rep.* **2013**, *3*, 1–7. [[CrossRef](#)]
77. Sinha, N.; Sen, S. Predicting hERG activities of compounds from their 3D structures: Development and evaluation of a global descriptors based QSAR model. *Eur. J. Med. Chem.* **2011**, *46*, 618–630. [[CrossRef](#)] [[PubMed](#)]
78. Perissinotti, L.L.; De Biase, P.M.; Guo, J.; Yang, P.-C.; Lee, M.C.; Clancy, C.E.; Duff, H.J.; Noskov, S.Y. Determinants of isoform-specific gating kinetics of hERG1 channel: Combined experimental and simulation study. *Front. Physiol.* **2018**, *9*, 207. [[CrossRef](#)]
79. Asai, T.; Adachi, N.; Moriya, T.; Oki, H.; Maru, T.; Kawasaki, M.; Suzuki, K.; Chen, S.; Ishii, R.; Yonemori, K. Cryo-EM structure of K⁺-bound hERG channel complexed with the blocker astemizole. *Structure* **2021**, *29*, 203–212.e204. [[CrossRef](#)]
80. Vanommeslaeghe, K.; Hatcher, E.; Acharya, C.; Kundu, S.; Zhong, S.; Shim, J.; Darian, E.; Guvench, O.; Lopes, P.; Vorobyov, I.; et al. CHARMM general force field: A force field for drug-like molecules compatible with the CHARMM all-atom additive biological force fields. *J. Comput. Chem.* **2010**, *31*, 671–690. [[CrossRef](#)]
81. Vanommeslaeghe, K.; MacKerell, A.D., Jr. Automation of the CHARMM General Force Field (CGenFF) I: Bond Perception and Atom Typing. *J. Chem. Inf. Model.* **2012**, *52*, 3144–3154. [[CrossRef](#)]
82. Vanommeslaeghe, K.; Raman, E.P.; MacKerell, A.D., Jr. Automation of the CHARMM General Force Field (CGenFF) II: Assignment of Bonded Parameters and Partial Atomic Charges. *J. Chem. Inf. Model.* **2012**, *52*, 3155–3168. [[CrossRef](#)] [[PubMed](#)]
83. Chemical Computing Group ULC. *Molecular Operating Environment MOE 2020.09*; Chemical Computing Group ULC: Montreal, QC, Canada, 2022.
84. Grisoni, F.; Ballabio, D.; Todeschini, R.; Consonni, V. Molecular descriptors for structure–activity applications: A hands-on approach. In *Computational Toxicology*; Springer: New York, NY, USA, 2018; pp. 3–53.
85. Mao, J.; Akhtar, J.; Zhang, X.; Sun, L.; Guan, S.; Li, X.; Chen, G.; Liu, J.; Jeon, H.-N.; Kim, M.S. Comprehensive strategies of machine-learning-based quantitative structure-activity relationship models. *Iscience* **2021**, *24*, 103052. [[CrossRef](#)] [[PubMed](#)]
86. Todeschini, R.; Consonni, V. *Handbook of Molecular Descriptors*. John Wiley & Sons: Hoboken, NJ, USA, 2008.
87. Pearlman, D.A.; Charifson, P.S. Are Free Energy Calculations Useful in Practice? A Comparison with Rapid Scoring Functions for the p38 MAP Kinase Protein System†. *J. Med. Chem.* **2001**, *44*, 3417–3423. [[CrossRef](#)] [[PubMed](#)]
88. Kalyaanamoorthy, S.; Barakat, K.H. Binding modes of hERG blockers: An unsolved mystery in the drug design arena. *Expert Opin. Drug Discov.* **2018**, *13*, 207–210. [[CrossRef](#)] [[PubMed](#)]
89. Chen, J.; Seeböhm, G.; Sanguinetti, M.C. Position of aromatic residues in the S6 domain, not inactivation, dictates cisapride sensitivity of HERG and eag potassium channels. *Prac. Natl. Acad. Sci. USA* **2002**, *99*, 12461–12466. [[CrossRef](#)] [[PubMed](#)]
90. Sanguinetti, M.C.; Tristani-Firouzi, M. hERG potassium channels and cardiac arrhythmia. *Nature* **2006**, *440*, 463–469. [[CrossRef](#)]
91. Saxena, P.; Zangerl-Plessl, E.-M.; Linder, T.; Windisch, A.; Hohaus, A.; Timin, E.; Hering, S.; Stary-Weinzinger, A. New potential binding determinant for hERG channel inhibitors. *Sci. Rep.* **2016**, *6*, 1–10. [[CrossRef](#)]
92. Sanguinetti, M.C.; Chen, J.; Fernandez, D.; Kamiyat, K.; Mitcheson, J.; Sanchez-Chapula, J.A. Physicochemical basis for binding and voltage-dependent block of hERG channels by structurally diverse drugs. In *The hERG Cardiac Potassium Channel: Structure, Function and Long QT Syndrome*; John Wiley & Sons: Hoboken, NJ, USA, 2005; p. 159.
93. Gillman, K.W.; Parker, M.F.; Silva, M.; Degnan, A.P.; Tora, G.O.; Lodge, N.J.; Li, Y.-W.; Lelas, S.; Taber, M.; Krause, R.G. Design, optimization, and in vivo evaluation of a series of pyridine derivatives with dual NK1 antagonism and SERT inhibition for the treatment of depression. *Bioorg. Med. Chem. Lett.* **2013**, *23*, 407–411. [[CrossRef](#)]
94. Durdagi, S.; Subbotina, J.; Lees-Miller, J.; Guo, J.; Duff, H.J.; Noskov, S.Y. Insights into the molecular mechanism of hERG1 channel activation and blockade by drugs. *Curr. Med. Chem.* **2010**, *17*, 3514–3532. [[CrossRef](#)]
95. Choe, H.; Nah, K.H.; Lee, S.N.; Lee, H.S.; Lee, H.S.; Jo, S.H.; Leem, C.H.; Jang, Y.J. A novel hypothesis for the binding mode of HERG channel blockers. *Biochem. Biophys. Res. Comm.* **2006**, *344*, 72–78. [[CrossRef](#)]
96. Miranda-Quintana, R.A.; Bajusz, D.; Rácz, A.; Héberger, K. Extended similarity indices: The benefits of comparing more than two objects simultaneously. Part 1: Theory and characteristics. *J. Cheminformatics* **2021**, *13*, 32. [[CrossRef](#)] [[PubMed](#)]

-
97. Miranda-Quintana, R.A.; RÁCZ, A.; Bajusz, D.; Héberger, K. Extended similarity indices: The benefits of comparing more than two objects simultaneously. Part 2: Speed, consistency, diversity selection. *J. Cheminformatics* **2021**, *13*, 33. [[CrossRef](#)] [[PubMed](#)]
 98. Dunn, T.B.; Seabra, G.M.; Kim, T.D.; Juárez-Mercado, K.E.; Li, C.; Medina-Franco, J.L.; Miranda-Quintana, R.A. Diversity and Chemical Library Networks of Large Data Sets. *J. Chem. Inf. Model.* **2021**, *in press*. [[CrossRef](#)] [[PubMed](#)]